

Skewness as a test of dark energy perturbations

Raquel Emy Fazolo*

PPGCosmo, Universidade Federal do Espírito Santo, 29075-910, Vitória, ES, Brazil

Luca Amendola†

*Institute of Theoretical Physics, Philosophenweg 16,
Heidelberg University, 69120, Heidelberg, Germany*

Hermano Velten‡

*Departamento de Física, Universidade Federal de Ouro Preto (UFOP),
Campus Morro do Cruzeiro, 35400-000, Ouro Preto-MG Brazil*

(Dated: June 12, 2025)

We investigate the role played by dark energy perturbations in the skewness S_3 of large-scale matter distribution. We consider a two-fluid universe composed by matter and dark energy, with perturbations in both components, and we estimate numerically the skewness of the matter density field as a function of the dark energy parameters. We characterize today's S_3 value for quintessence and phantom dark energy cosmologies as well as its dependence on the matter density parameter Ω_{m0} and the dark energy sound speed c_s^2 with accurate numerical fitting. These fits can be used to test cosmology against future high quality data on large scale structure.

Keywords: Cosmology, dark energy, large scale structure, cosmological perturbations

I. INTRODUCTION

Observations show that today's universe is composed mostly of dark energy ($\approx 70\%$), a substance responsible for the current accelerated expansion which also, under normal circumstances, slows down the clustering of the universe's matter content. As well known, the simplest form of dark energy is a constant Λ in Einstein's general relativity acting only at expanding background level. A fluid model for dark energy is however also a valid description allowing for a time evolution of its energy density. The implementation of the fluid formalism demands the definition of an equation of state parameter (EoS), $w = P/\rho$, defined as the ratio of the fluid's pressure P and its energy density ρ . For the dark energy case, even though a time evolving EoS parameter provides a vast collection of possible dynamical scenarios, a constant w is enough to produce a rich phenomenology of dark energy models.

In a first approximation, the late-time universe can be described as a homogeneous and isotropic expanding background filled with matter and dark energy. Aspects of large scale structure are studied mainly via the definition of the matter density contrast $\delta\rho_m$ and dark energy perturbations are usually neglected or are shown not to be able to contribute to the linear regime of structure formation [1]. The latter assumption is formally obeyed by a cosmological constant since it does not cluster and, to a good approximation, by time-evolving dark energy models with speed of sound close to unity [2–8]. On the other hand, dark energy perturbations in nonadiabatic dark energy models are severely constrained by observations [9].

While the role played by dark energy perturbations at first order has been widely studied in the literature [10–14], dark energy effects at higher clustering perturbative orders are still poorly explored: for example, and more specifically for the goal of this work, the effects of dark energy perturbation on the skewness (S_3) of the matter density. The skewness, defined as the normalized third order moment of the counts-in-cells statistics, can be used to evaluate asymmetric features in the probability distribution function (PDF) of the matter clustering field. A finite skewness indicates the existence of a non-vanishing balance between clustering and voids in the large scale structure distribution. Indeed, it is well known that the cosmological gravitational clustering process yields to a skewed large scale structure [15, 16]. In a fully matter-dominated universe (the Einstein-de Sitter model), one finds the well-known result $S_3 \simeq 34/7 \simeq 4.857$ [16, 17], to be corrected for finite-volume effects.

In previous work [18], by following the treatment used in Ref. [19], dark energy effects on S_3 have been studied by modelling the entire cosmic substratum, i.e., matter and dark energy, as a single fluid. By encoding dark energy effects into an effective equation of state and an effective speed of sound for the total matter fluid, a significant increase

* raquel.fazolo@edu.ufes.br

† l.amendola@thphys.uni-heidelberg.de

‡ hermano.velten@ufop.edu.br

of the skewness value ($S_3 \sim 15$) was found for any dynamical dark energy model while skewness for Λ CDM model remains close to $34/7$. This result, while still employing a simplistic treatment, has showed that the skewness S_3 is a promising test to identify cosmic signatures of dark energy perturbations. While being an interesting cosmological observable, the actual S_3 value is still poorly constrained by the current observations [20] but in the near future, with surveys like Euclid [21, 22], a reliable map the three-dimensional matter distribution of the universe can provide an accurate measurement of S_3 . On the other hand, large scale N-body simulations can be used to investigate skewness as done recently in Ref. [23].

Our aim with this work is to continue the search for dark energy signatures on the skewness of matter distribution. Now, going beyond the analysis performed in Ref. [18], we fully take into account fluctuations in both cosmological fluids using the perturbed equations up to second order for a universe composed by matter and dark energy. The dark energy density contrast acts as an independent source of the matter fluctuations.

The main product of this paper is embodied in a series of numerical fitting formulas for the S_3 value calculated as a function of Ω_{m0} and w_{de} , with different choices of the dark energy sound speed c_s^2 . These fits might be useful when forecoming high-precision data from large scale structure surveys will be able to measure S_3 to a percent precision. We expand over previous results in several ways: *a*) we include the dark energy perturbations; *b*) we simultaneously fit for Ω_{m0} and w_{de} ; *c*) we adopt different values for c_s^2 . The main equations of our work are presented in the next section. In the third section we provide the numerical analysis and the fitting formulas for S_3 . We conclude in the final section.

II. BACKGROUND AND PERTURBED DYNAMICS

Since we focus on the late time cosmological dynamics (where the radiation contribution is negligible), we consider a non-interacting two-fluid model composed by pressureless matter $P_m = 0$ (subscript m) and dark energy with pressure $P_{de} = w_{de}\rho_{de}$ (subscript de). In a general-relativistic based description of the gravitational interaction sourced by matter and dark energy, Einstein's equations take the form

$$R_{\mu\nu} - \frac{1}{2}g_{\mu\nu}\mathcal{R} = 8\pi GT_{(m)\mu\nu} + 8\pi GT_{(de)\mu\nu}, \quad (1)$$

being $R_{\mu\nu}$ the Ricci tensor and $\mathcal{R} = g^{\mu\nu}R_{\mu\nu}$ the Ricci scalar. Both components are described by a perfect fluid energy momentum tensor. Using the background expansion rate of a flat, homogeneous and isotropic universe - the Friedmann-Lemaître-Robertson-Walker (FLRW) metric - one finds

$$\frac{H^2}{H_0^2} = \Omega_{m0}a^{-3} + \Omega_{de0}e^{-3\int da\frac{1+w_{de}}{a}}. \quad (2)$$

where $H = \dot{a}/a$ is the Hubble expansion rate parameter, a dot represents the derivative with respect to cosmic time, and the scale factor is normalized to the present value $a_0 = 1$. Since we assume a flat universe, we have $\Omega_{de0} = 1 - \Omega_{m0}$.

Let us now focus on the cosmological perturbation analysis needed to calculate the skewness of matter distribution. Since on sub-horizon scales Newtonian physics describes fairly well the cosmological expansion and its perturbations, we restrict our formalism to a post-Newtonian approach, or neo-Newtonian, as e.g. in [24, 25]. Then, within the fluid limit, the cosmological dynamics can be recast in the form of a hydrodynamical system with velocity field given by the Hubble's law $\vec{u} = H\vec{r}$. In this formalism energy conservation is expressed in terms of the following continuity equation [24]

$$\left(\frac{\partial \rho}{\partial t} \right)_r + \vec{\nabla}_r \cdot (\rho \vec{u}) + P \vec{\nabla}_r \cdot \vec{u} = 0. \quad (3)$$

The momentum conservation of a fluid moving under the influence of the gravitational field ϕ is represented by the Euler equation

$$\left(\frac{\partial \vec{u}}{\partial t} \right)_r + (\vec{u} \cdot \vec{\nabla}_r) \vec{u} = -\vec{\nabla}_r \phi - (\rho + P)^{-1} \vec{\nabla}_r P. \quad (4)$$

It is worth noting that we are going to neglect shear and vorticity in the Euler equation, a widely-employed approximation that allows our resulting set of equations to be closed.

Each individual fluid obeys equations (3) and (4). In the case of a N -fluid system, the entire dynamics will be given by $2N$ equations sourced by the function ϕ , i.e., $2N + 1$ variables. Thus, the system of equations will be closed by

considering the Poisson equation (in the neo-Newtonian cosmology) relating the gravitational field to the contribution of the components such that

$$\nabla^2\phi = 4\pi G(\rho + 3P). \quad (5)$$

For a system composed by $N = 2$ components, i.e. matter and dark energy, we end up with a set of 5 equations. This post-Newtonian approach allows one to obtain the relativistic Friedmann Eq. (2) with the identification $\vec{u} = H\vec{r}$.

Now, in order to assess the statistical moments of the matter density field, we introduce small perturbations around the background quantities, i.e.,

$$\begin{aligned} \rho &= \rho_0 + \delta\rho, \\ P &= P_0 + \delta P, \\ \phi &= \phi_0 + \varphi, \\ \vec{u} &= \vec{u}_0 + \vec{v}. \end{aligned} \quad (6)$$

It is also convenient to adopt the comoving coordinates \vec{x} such that

$$\begin{aligned} \vec{r} &= a\vec{x}, & \vec{\nabla}_x &= a\vec{\nabla}_r, \\ \left(\frac{\partial f(\vec{x}, t)}{\partial t}\right)_r &= \left(\frac{\partial f}{\partial t}\right)_x - \frac{\dot{a}}{a}(\vec{x} \cdot \vec{\nabla}_x)f, \\ \vec{u} &= \dot{a}\vec{x} + \vec{v}(\vec{x}, t). \end{aligned}$$

Focusing on the scalar modes of the cosmological perturbations that are necessary to calculate the skewness of the matter density field one has to keep terms up to second order in the perturbed expansion. We proceed by isolating the divergence of the velocity field term in the perturbed continuity Eq. (3) and inserting it into Eq. (4). With this procedure we find the following equation for the density contrast $\delta = \delta\rho/\rho$

$$\begin{aligned} \delta'' + \delta' &\left[3(c_s^2 - w) + \left(1 + \frac{\mathcal{H}'}{\mathcal{H}}\right) - \frac{w'}{1 + w + (1 + c_s^2)\delta} \right] - \delta'^2 \left[\frac{4/3 + c_s^2}{1 + w + (1 + c_s^2)\delta} \right] \\ &+ \delta\delta' \left[\frac{(w - c_s^2)(5 + 3c_s^2) - c_s'^2}{1 + w + (1 + c_s^2)\delta} \right] + \delta^2 \left[\frac{3(w - c_s^2)c_s'^2 + 3(w - c_s^2)^2}{1 + w + (1 + c_s^2)\delta} \right] \\ &+ 3\delta \left[(c_s'^2 - w') + \left(1 + \frac{\mathcal{H}'}{\mathcal{H}}\right)(c_s^2 - w) + \frac{w'(w - c_s^2)}{1 + w + (1 + c_s^2)\delta} \right] \\ &+ \frac{1 + w + (1 + c_s^2)\delta}{\mathcal{H}^2} \nabla^2\varphi = \frac{1 + w + (1 + c_s^2)\delta}{\mathcal{H}^2} \nabla \left[\frac{\nabla(c_s^2\delta)}{1 + w + (1 + c_s^2)\delta} \right], \end{aligned} \quad (7)$$

where the prime represents a derivative with respect to $N = \ln(a)$ and $\mathcal{H} = a'/a$. Eq. (7) represents the most general equation for the evolution of the density contrast of a fluid with effective speed of sound given by $c_s^2 = \delta P/\delta\rho$ sourced by a gravitational potential φ .

Let us now apply Eq. (7) to the matter fluid. In the case of a pressureless component both the equation of state parameter and the speed of sound vanish i.e., $w_m = c_{s(m)}^2 = 0$, and therefore Eq. (7) reduces to the well-known equation

$$\delta_m'' + \delta_m' \left(1 + \frac{\mathcal{H}'}{\mathcal{H}}\right) - \delta_m'^2 \left(\frac{4/3}{1 + \delta_m}\right) + (1 + \delta_m) \frac{\nabla^2\varphi}{\mathcal{H}^2} = 0. \quad (8)$$

The contribution of the gravitational potential φ is provided by the perturbed Poisson equation. If the universe is filled with both pressureless matter and dark energy, the perturbed Poisson equation reads

$$\nabla^2\varphi = -\frac{3}{2}\Omega_m\mathcal{H}^2\delta_m - \frac{3}{2}\Omega_{de}\mathcal{H}^2 \left[1 + 3c_{s(de)}^2\right] \delta_{de}. \quad (9)$$

Hereafter we use the simplified notation $c_{s(de)}^2 \equiv c_{de}^2$ for the effective dark energy speed of sound. We will treat c_{de}^2 as a constant free parameter in our analysis. At this point one can notice that all dark energy perturbations effects on the gravitational potential can be eliminated by setting $c_{de}^2 = -1/3$. However, of course, this choice does not represent a realistic dark energy fluid.

In order to decouple Eq. (8) into first order and second order contributions, we expand the matter density contrast in terms of the growth functions D_i [15, 16]

$$\delta_m = \sum_{i=1}^{\infty} \delta_i = \sum_{i=1}^{\infty} \frac{D_i(\eta)}{i!} \delta_0^i \simeq D_1 \delta_0 + \frac{D_2}{2} \delta_0^2 + \mathcal{O}(\delta_0^3), \quad (10)$$

where δ_0 is the density contrast at some initial epoch. By neglecting $\mathcal{O}(\delta_0^3)$ terms in the above sum the resulting dynamics is given by two equations for the evolution of the first order (D_1) and second order (D_2) growth functions. They read, respectively,

$$D_1'' + D_1' \left(1 + \frac{\mathcal{H}'}{\mathcal{H}} \right) - \frac{3}{2} D_1 \Omega_m - \frac{3}{2} \Omega_{de} \delta_{de} (1 + 3c_{de}^2) = 0, \quad (11)$$

$$D_2'' + D_2' \left(1 + \frac{\mathcal{H}'}{\mathcal{H}} \right) - \frac{8}{3} D_2^2 - \frac{3}{2} D_2 \Omega_m - 3D_1^2 \Omega_m - 3D_1 \Omega_{de} \delta_{de} (1 + 3c_{de}^2) = 0. \quad (12)$$

The dark energy perturbation terms can be easily identified in the above equations. They can be switched off by setting $\delta_{de} = 0$. Notice that we kept δ_{de} at first order because dark energy is expected to be much less clustered than matter.

With these equations we can finally calculate the skewness S_3 , defined as [16]

$$S_3 = \frac{3D_2}{D_1^2}. \quad (13)$$

We now calculate S_3 in the case the matter density field is sourced by the dark energy fluctuations δ_{de} . The evolution of the latter is obtained by adapting Eq. (7) to the dark energy fluid. Since Eqs. (11) and (12) are sourced by the first order dark energy density perturbation δ_{de} , we also have to provide its linear equation in Fourier space

$$\begin{aligned} \delta_{de}'' + \delta_{de}' & \left[3(c_{de}^2 - w_{de}) + \left(1 + \frac{\mathcal{H}'}{\mathcal{H}} \right) - \frac{w_{de}'}{1 + w_{de}} \right] \\ & + 3\delta_{de} \left[(c_{de}^{2\prime} - w_{de}') + \left(1 + \frac{\mathcal{H}'}{\mathcal{H}} \right) (c_{de}^2 - w_{de}) - \frac{w_{de}'(c_{de}^2 - w_{de})}{1 + w_{de}} \right] \\ & - (1 + w_{de}) \frac{3}{2} [\Omega_m D_1 + \Omega_{de} (1 + 3c_{de}^2) \delta_{de}] + \frac{c_{de}^2 k^2}{\mathcal{H}^2} \delta_{de} = 0. \end{aligned} \quad (14)$$

When dark energy perturbations are included, a dependence on the wavenumber k appears in Eq. (14). We have checked however that S_3 is very weakly dependent on the k -value for the range of scales of cosmological interest, with changes by at most 10^{-5} . Therefore we neglect the k -dependence and adopt for all results the scale $k = 0.1 h/\text{Mpc}$, close to the range of scales effectively observed in large-scale surveys.

The dark energy speed of sound c_{de}^2 will be taken as an additional free parameter. Hereafter we will adopt the following values

- $c_{de}^2 = 0$, a situation in which dark energy perturbation follows the behavior of the pressureless-like clustering fluid;
- $c_{de}^2 = 1$, the effective speed of sound of a scalar field component;
- $c_{de}^2 = 1/3$, as indicated recently by the analysis of Ref. [26].

The analysis of [26] refers to a model different from the one of this work, but suggests the possibility of a dark energy model with a preferred sound speed different from zero or unity, so we adopt this value for qualitative purposes. Finally, besides giving accurate fits for these values, we also include c_{de}^2 as a third parameter along with Ω_{m0} and w_{de} .

III. RESULTS AND NUMERICAL FITS

An expansion for the skewness value around the Einstein-De-Sitter universe ($\Omega_m = 1$ and $\Omega_\Lambda = 0$) is often employed in the literature. A widely known result is provided by Bernardeau et al. (2002) [16] where a weak dependence of the skewness on the Ω_{m0} parameter $S_3 = 34/7 + 6/7(\Omega_{m0}^{-0.03} - 1)$ has been found for the case where $\Lambda = 0$. The main

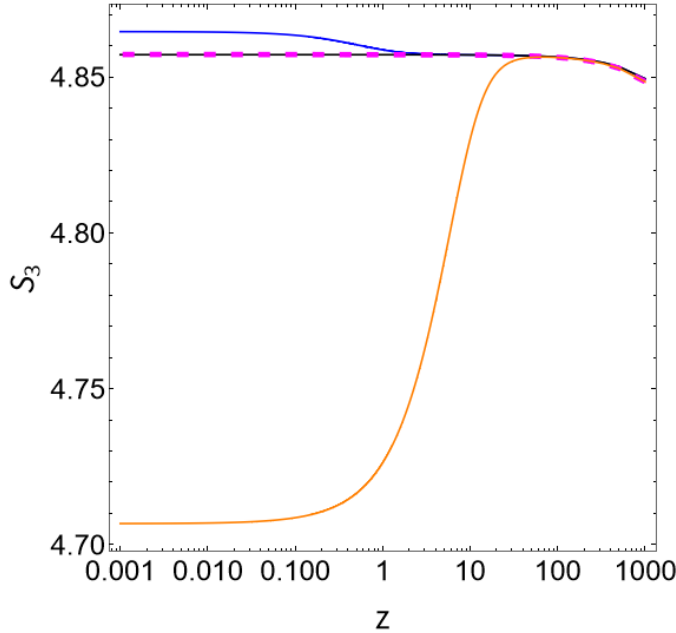


FIG. 1. Skewness evolution as a function of redshift. The colors represent the following cases: blue for a Λ CDM case i.e., $\Omega_{m0} = 0.3$, $w_{de} = -1$; black for EdS case i.e., $\Omega_{m0} = 1$ and $c_{de}^2 = 0$; orange for the quintessence case with $\Omega_{m0} = 0.3$, $w_{de} = -0.8$ and $c_{de}^2 = 1$ and finally the dashed magenta for a phantom case with $\Omega_{m0} = 0.3$, $w_{de} = -1.2$ and $c_{de}^2 = 1$, the last two includes dark energy perturbations. The black line and the dashed magenta are almost indistinguishable.

goal of this paper is to extend this analysis by including the effects of dark energy fluctuations as a function of the matter density parameter Ω_{m0} , the dark energy equation of state w_{de} , and its squared sound speed c_{de}^2 .

We begin our analysis by showing in Fig. 1 how the skewness evolves in time for a Λ CDM cosmology with parameters $\Omega_{m0} = 0.3$, $w_{de} = -1$ (blue line) and for the Einstein-de Sitter (EdS) model (black line). As expected, the non-Gaussianity increases with time reaching asymptotically a constant value for both cases. One can clearly see the manifestation of dark energy around redshift 1. We also show models with dark energy perturbations for $w_{de} = -0.8$ and $w_{de} = -1.2$.

Next, we compare S_3 with and without dark energy perturbations. We solve numerically Eq. (11), Eq. (12), and Eq. (14) varying the parameters Ω_{m0} and w_0 . We choose $a_i = 1/(1+z_i)$, being $z_i \simeq 300000$ such as when $t \rightarrow 0$ we have EdS values [15], our initial condition and also assume $D_1(a_i) \propto a$ and $D_2(a_i) \propto a^2$. We show in Fig. 2 today's skewness value S_3 as a function of Ω_{m0} for various values of w_{de} and c_{de}^2 . On the left plot of Fig. 2 we notice that for the quintessence cases ($w_{de} = -0.9$ in the figure) the inclusion of dark energy perturbations has a relatively large impact. We find that dark energy perturbations always lower the skewness with respect to $\delta_{de} = 0$. As for phantom cases ($w_{de} = -1.2$ in plot), we find almost no change. This seems to indicate that the skewness can be a much better tool to test quintessence models than for models in the phantom regime. Also the speed of sound for the dark energy fluid affects the skewness in different ways depending on whether dark energy is phantom [27] or quintessence [28] as also shown in Fig. 2. Overall, we see that the typical change in S_3 from model to model is of the order of 1 or 2%.

In order to provide an expression for S_3 as a function of the cosmological parameters, we have performed phenomenological fits to the numerical results. To assess the quality of the fits, we adopt two measures, the maximum relative deviation (MRD) and the average standard relative deviation (ASRD), defined respectively as the following percentages

$$\begin{aligned} \text{MRD} &= 100 \text{ Max} \left| \frac{\text{Fit}(i) - \text{Data}(i)}{\text{Fit}(i)} \right|, \\ \text{ASRD} &= 100 \sqrt{\frac{1}{N} \sum \left(\frac{\text{Fit}(i) - \text{Data}(i)}{\text{Fit}(i)} \right)^2}, \end{aligned} \quad (15)$$

where $\text{Data}(i)$ represents the numerical outcomes of our system of equations for a given set parameter values i and $\text{Fit}(i)$ is the fitted function.

In Fig. 2 (right side) we show that the skewness calculated for a Λ CDM ($\delta_{de} = 0$) case is almost identical to

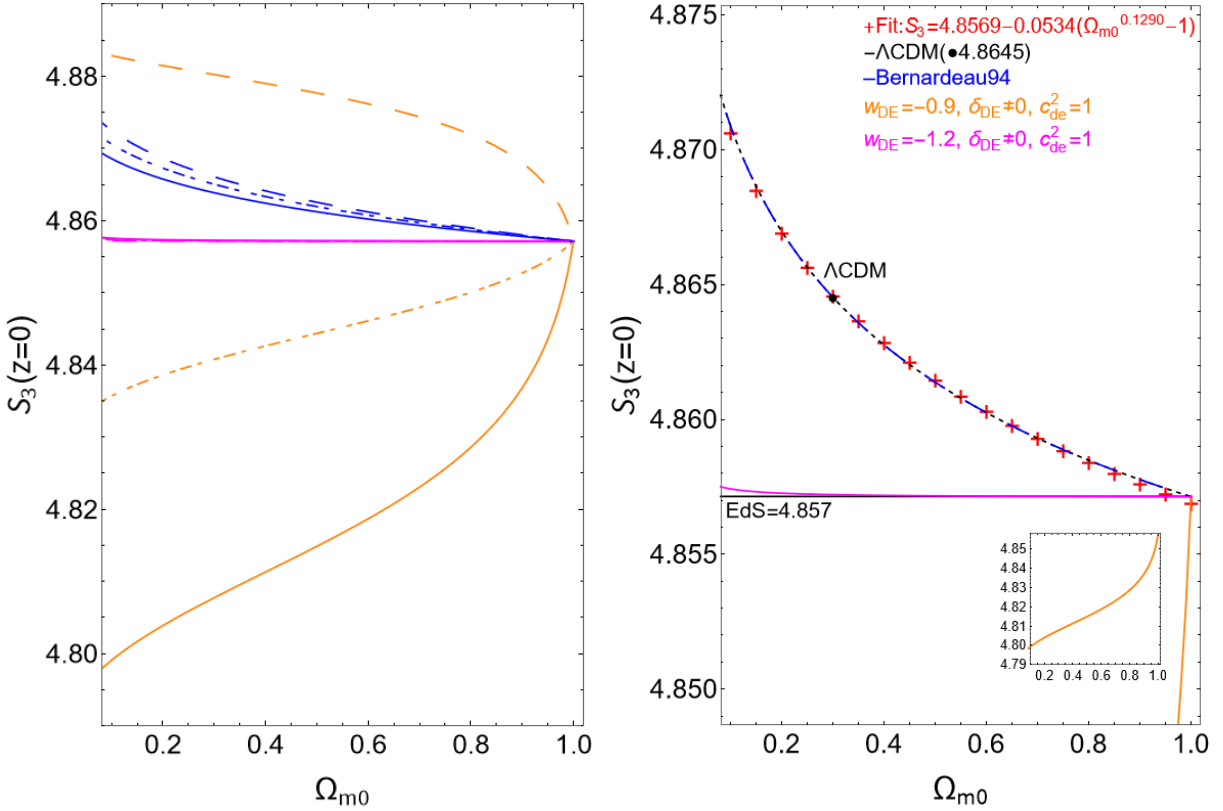


FIG. 2. Dependence of the skewness on the density parameter Ω_{m0} . In the left panel the dot-dashed lines represent $c_{de}^2 = 0$, solid lines $c_{de}^2 = 1$ and dashed lines is the case without dark energy perturbations ($\delta_{de} = 0$). The colors refers to different w_{de} values: blue for $w_{de} = -1$, magenta for $w_{de} = -1.2$ and orange for $w_{de} = -0.9$. On the right side we show the skewness for $\Lambda \neq 0$ by Bernardeau (1994) [15] (dashed blue) compared to our result (dashed black) for the Λ CDM case ($w_{de} = -1$, $\Omega_{m0} = 0.3$ (black dot) and no dark energy perturbations $\delta_{de} = 0$). The black line is for the EdS skewness value of $34/7 = 4.857$. The fit Eq.(16) is represented by the red cross symbols. We also show the skewness when dark energy perturbations are included, for $w_{de} = -0.9$ (orange) $w_{de} = -1.2$ (magenta), both with $c_{de}^2 = 1$. The inset in the right panel shows the full behavior of the $w_{de} = -0.9$ case.

Bernardeau's results in [15] for $\Lambda \neq 0$. A fit to our results is provided as the following equation:

$$S_3 = 4.857 - 0.053(\Omega_{m0}^{0.129} - 1). \quad (16)$$

For this fit we obtain the following values quality measurements: MRD=0.01% and ASRD= 0.002% compared to the results of the equations itself. We also plot in the same figure the EdS reference value $34/7 = 4.857$ as the horizontal black line and repeat the cases for dynamical dark energy models for quintessence $w_{de} = -0.9$ and phantom $w_{de} = -1.2$ cosmologies including dark energy perturbations, both with $c_{de}^2 = 1$ as in the left panel.

As already mentioned, the skewness depends much more strongly on w_{de} in the regime $w_{de} > -1$ than below it (i.e., in the phantom regime), as shown more clearly in Fig. 3.

Our goal now is to obtain a general fitting formula for S_3 that includes the dependence on both Ω_{m0} and w_{de} for various values of c_{de}^2 . We propose the following parametrization, defined by six constants a, b, \dots, f :

$$S_3(\text{fit}) = a + b(\Omega_{m0}^c - 1) + d|(1 + w_{de})|^e + f(1 + \Omega_{m0}w_{de}). \quad (17)$$

By setting $d = e = f = 0$ one obtains the previous formula (16). Also, the constant S_3 value of the EdS model is immediately retrieved in the limit $\Omega_{m0} = 1$ and $w_{de} = -1$. We aim at an average (ASRD) and maximum (MRD) precision much better than 1% across the entire parametric range.

Tables I (phantom regime only) and II (quintessence regime only) report the values for the fitting free parameters a, b, \dots, f and their respective MRD and ASRD values for some values of c_{de}^2 . Although the ASRD is always much smaller than 1%, the MRD is larger for the quintessence regime, but we find that the deviation mostly occurs near the boundary regions of Ω_{m0} . So we also present in Tab. III the results for a smaller range of Ω_{m0} ($0.15 \leq \Omega_{m0} \leq 0.45$), obtaining improved fits.

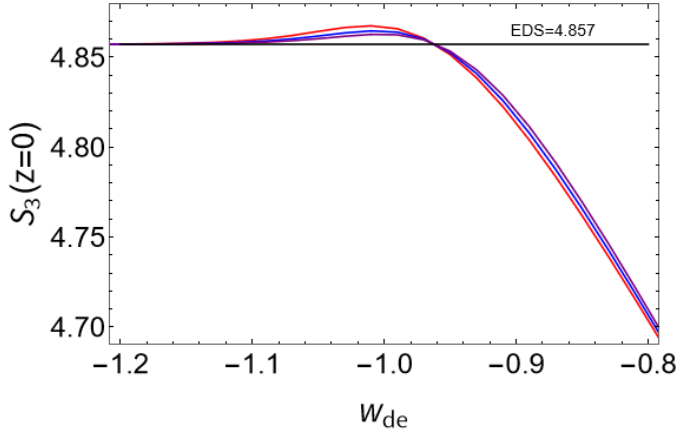


FIG. 3. Dependence of S_3 on the dark energy equation of state w_{de} . The colored curves refers to different values of the matter density parameter, namely $\Omega_{m0} = 0.2$ (red), $\Omega_{m0} = 0.3$ (blue) and $\Omega_{m0} = 0.4$ (purple). The black line sets the Einstein-de Sitter value $34/7$. We assumed $c_{de}^2 = 1$ for all curves.

Phantom ($-1.25 \leq w_{de} \leq -1$)	a	b	c	d	e	f	MRD%	ASRD%
$c_{de}^2 = 0$	4.861	-0.052	0.908	-0.023	0.444	-0.042	0.06	0.01
$c_{de}^2 = 1$	4.860	-0.067	0.899	-0.030	0.552	-0.053	0.08	0.01
$c_{de}^2 = 1/3$	4.860	-0.059	0.903	-0.026	0.500	-0.047	0.07	0.01

TABLE I. Fit values for Eq. (17) for the phantom regime $-1.25 \leq w_{de} \leq -1$.

In order to visualise the accuracy of the fitting formula Eq.(17) with the parameters of Table(II), we show in Fig.4 the comparison between the numerically generated data and the fit. Here we have chosen to display the quintessence case; since this is the case with largest MRD and ASRD values, all other parameter configurations produce a better fit.

We also propose a general fitting formula with c_{de}^2 as a variable [29–31]. The results are presented in Table(IV) and Fig.(5):

$$S_3(\text{fit-}c_{de}^2) = a + b(\Omega_{m0}^c - 1) + d|(1 + w_{de})|^e + f(1 + \Omega_{m0}w_{de}) + g(c_{de}^2 + w_{de}). \quad (18)$$

We can see from Table (I) that c_{de}^2 has a very little effect in the phantom regime. For example for $w_{de} = -1.10$ and $\Omega_{m0} = 0.3$, one has a slight increase of only 0.01% in the S_3 value when c_{de}^2 varies from 0 to 1. The impact is larger in the quintessence regime Table (II): for instance, for $w_{de} = -0.90$ and $\Omega_{m0} = 0.3$, when c_{de}^2 varies from 0 to 1, we have a decrease of 0.5% in the S_3 value.

Apart from the theoretical analysis performed so far, it is also important to have contact with observed quantities. However, the value of S_3 for biased tracers is actually expected to be shifted by a factor and a constant that depend on the linear and non-linear bias parameters [32], plus a correction that depends on the cell window function. One could compare the data with S_3 and find the best fit values of the bias parameters, but here we limit ourselves to plotting S_3 against the data to have a general idea of the trend.

In Fig. 6 we show our results against the observed values from Ref. [20] from the CFHTLS-Wide survey. In this analysis the skewness is calculated using a counts-in-cells technique for several intervals of redshift. Here we managed to reproduce a larger range of theoretical results than in [20] using a well-behaved (i.e., less oscillating than the top-hat) window function, namely

$$W(kR) = \frac{\sqrt{2}e^{-\frac{kR}{\sqrt{2}}}}{kR} \sin\left(\frac{kR}{\sqrt{2}}\right), \quad (19)$$

Quintessence ($-1 \leq w_{de} \leq -0.8$)	a	b	c	d	e	f	MRD%	ASRD%
$c_{de}^2 = 0$	4.852	0.334	1.076	-2.534	1.924	0.364	1.12	0.06
$c_{de}^2 = 1$	4.861	0.437	1.138	-2.948	1.699	0.468	2.23	0.14
$c_{de}^2 = 1/3$	4.856	0.405	1.109	-2.841	1.791	0.437	1.72	0.11

TABLE II. Fit values for Eq. (17) for the quintessence regime $-1 \leq w_{de} \leq -0.8$.

Quintessence ($-1 \leq w_{de} \leq -0.8$) ($0.15 \leq \Omega_{m0} \leq 0.45$)	a	b	c	d	e	f	MRD%	ASRD%
$c_{de}^2 = 0$	4.853	0.244	0.986	-2.290	1.905	0.261	0.07	0.02
$c_{de}^2 = 1$	4.863	0.237	0.981	-2.321	1.605	0.240	0.11	0.03
$c_{de}^2 = 1/3$	4.858	0.250	0.982	-2.362	1.729	0.260	0.09	0.02

TABLE III. Fit values for Eq. (17) for the quintessence regime $-1 \leq w_{de} \leq -0.8$ but made for a smaller range of Ω_{m0} .

	a	b	c	d	e	f	g	MRD%	ASRD%
Phantom ($-1.25 \leq w_{de} \leq -1$)	4.860	-0.061	0.903	-0.027	0.510	-0.049	0.000	0.01	0.06
Quintessence ($-1 \leq w_{de} \leq -0.8$)	4.844	0.408	1.115	-2.854	1.794	0.439	-0.028	0.21	0.19

TABLE IV. Fit values for Eq. (18) for the phantom and quintessence regimes.

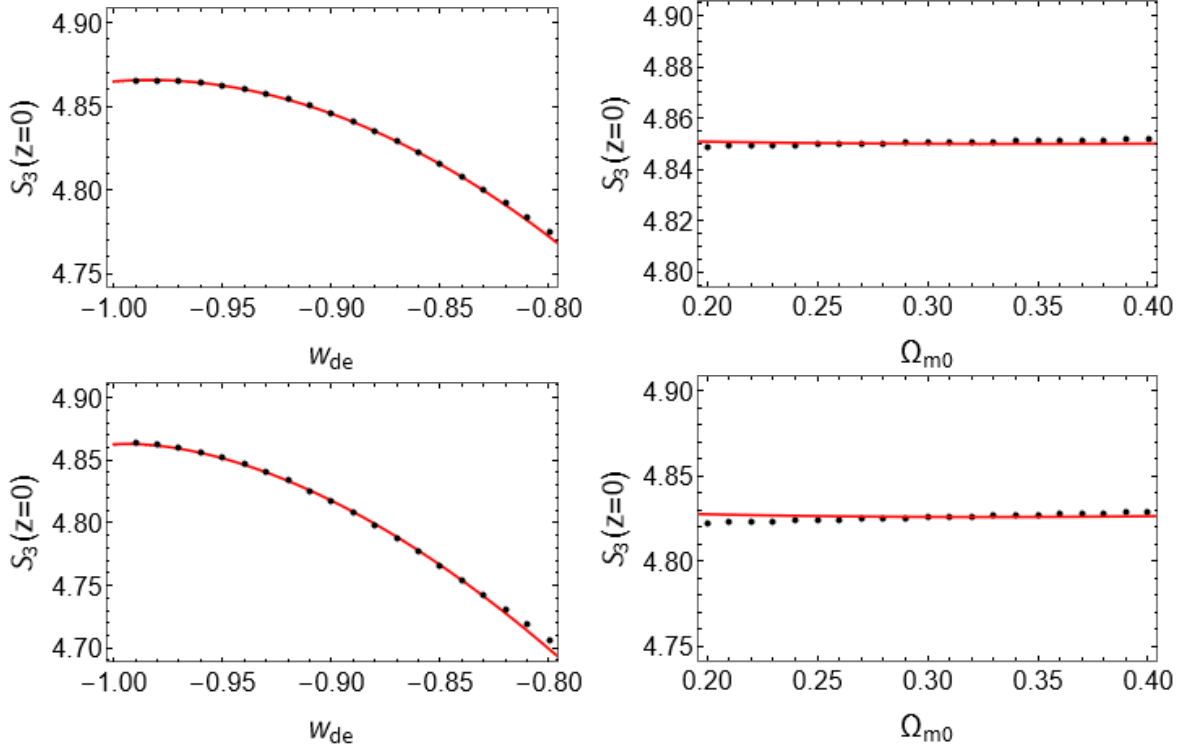


FIG. 4. Variation of skewness with Ω_{m0} and w_{de} . On the left panels we fix $\Omega_{m0} = 0.3$; on the right panels we fix $w_{de} = -0.9$. The red line represents the fit from Eq. (17) and Table II, and the black dots the data. Here we have the case for $c_{de}^2 = 0$ (top row) and $c_{de}^2 = 1$ (lower row).

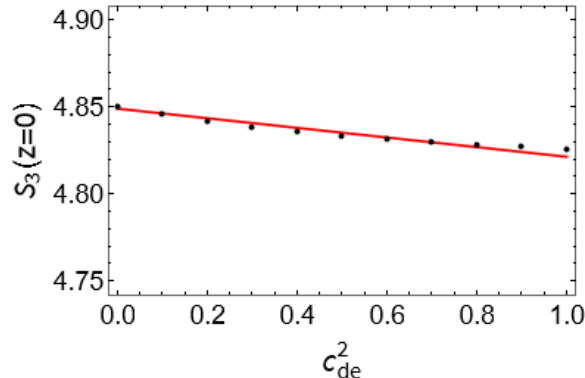


FIG. 5. Variation of skewness with c_{de}^2 . The red line represents the fit Eq.(18) and Table IV for $\Omega_{m0} = 0.3$ and $w_{de} = -0.9$; the black dots are the data.

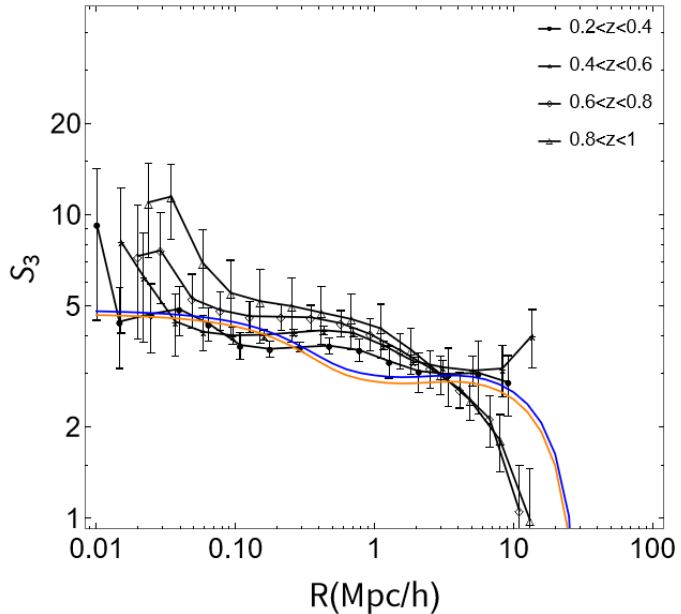


FIG. 6. Skewness compared to observational data from [20]. The blue line represents the theoretical plot using our set of equations with $\Omega_{m0} = 0.27$, $w_{de} = -1$, $c_{de}^2 = 0$ and $H_0 = 71$ km/s/Mpc that was also used in [20]. The orange line represents quintessence $w_{de} = -0.8$ and $c_{de}^2 = 1$. For the phantom case $w_{de} = -1.2$ and $c_{de}^2 = 1$, the curve is almost identical to the blue line. The theoretical curve is almost independent of z ; we plot here the $z = 0.9$ case.

where $W(kR)$ is the Fourier transform of the smoothed top-hat spherically symmetric region with characteristic radius R defined as $W(r) = 1/(1 + (r/R)^4)$ normalized to unity. Then, the following expression is used [16, 20, 33, 34]

$$S_3 = \frac{34}{7} + \gamma_1. \quad (20)$$

where $\gamma_1 = d \ln \sigma^2(R) / d \ln R$ is the count-in-cells correction [15, 20] and the variance of the density field in real space is given by

$$\sigma^2(R) = \frac{1}{2\pi^2} \int P(k, z) W^2(kR) k^2 dk. \quad (21)$$

where $P(k, z)$ is a Λ CDM power spectrum at redshift z . We can see that the general trend is consistent with the data, but clearly the precision is still far from allowing a robust constraint on the cosmological and the bias parameters.

IV. CONCLUSIONS

This work presents numerical estimates of S_3 (the third moment of the matter density field) when including dark energy perturbations while varying Ω_{m0} , w_{de} and c_{de}^2 . Whereas a cosmological constant affects the matter clustering features only via the background expansion, a dynamical dark energy field with its associated perturbations can lead to noticeable imprints on the large scale structure. This means that a measure of S_3 within a precision of 1% can put new constraints on cosmological parameters.

In a previous work, [18], the universe content was modeled as a effective single fluid (an admixture of dark energy and matter), in which the dark energy contributions have been considered via the total (the single fluid realization) equation of state parameter and sound speed. In contrast, in this work we consider the universe as composed by two separated fluids, both of which being perturbed. As expected, we obtain now values for today's S_3 much closer to the Λ CDM case (a factor of three smaller than in [18]), in agreement therefore with standard results presented in the literature, e.g. [15] and [20].

We found clear differences in the trend for quintessence ($w_{de} > -1$) and phantom models ($w_{de} < -1$), being S_3 more sensitive to the dark energy equation of state in the quintessence regime. This allows in principle to use the skewness to test cosmological models with $w_{de} > -1$.

We provided several fitting formulas accurate to within (or better than) 0.1% on average for S_3 as a function of the cosmological parameters Ω_{m0} , w_{de} and c_{de}^2 . These fits may be useful to compare the cosmological models to large scale structure at higher orders.

In future work, we plan to extend this analysis to include more cosmological parameters and modified gravitational models, as e.g. in [35, 36].

ACKNOWLEDGMENTS

Raquel Fazolo thanks CNPq and FAPES for financial support. Hermano Velten thanks CAPES/CNPq and Proppi/UFOP for partial financial support. LA acknowledges financial support from DFG project 456622116.

[1] Luca Amendola. Linear and non-linear perturbations in dark energy models. *Phys. Rev. D*, 69:103524, 2004.

[2] L. R. Abramo, R. C. Batista, L. Liberato, and R. Rosenfeld. Structure formation in the presence of dark energy perturbations. *JCAP*, 11:012, 2007.

[3] L. R. Abramo, R. C. Batista, L. Liberato, and R. Rosenfeld. Physical approximations for the nonlinear evolution of perturbations in inhomogeneous dark energy scenarios. *Phys. Rev. D*, 79:023516, 2009.

[4] D. F. Mota and C. van de Bruck. On the Spherical collapse model in dark energy cosmologies. *Astron. Astrophys.*, 421:71–81, 2004.

[5] Ronaldo C. Batista and Valerio Marra. Clustering dark energy and halo abundances. *JCAP*, 11:048, 2017.

[6] Matteo Fasiello and Zvonimir Vlah. Nonlinear fields in generalized cosmologies. *Phys. Rev. D*, 94(6):063516, 2016.

[7] Emiliano Sefusatti and Filippo Vernizzi. Cosmological structure formation with clustering quintessence. *JCAP*, 03:047, 2011.

[8] Takao Endo, Atsushi J. Nishizawa, and Kiyotomo Ichiki. Effect of dark energy perturbation on cosmic voids formation. *Mon. Not. Roy. Astron. Soc.*, 478(4):5230–5239, 2018.

[9] Winfried Zimdahl, Júlio Fabris, Hermano Velten, and Ramón Herrera. On (non-)dynamical dark energy. *Phys. Dark Univ.*, 30:100681, 2020.

[10] Manvendra Pratap Rajvanshi and J. S. Bagla. Nonlinear spherical perturbations in Quintessence Models of Dark Energy. *JCAP*, 06:018, 2018. [Erratum: *JCAP* 03, E01 (2020)].

[11] F. Pace, C. Fedeli, L. Moscardini, and M. Bartelmann. Structure formation in cosmologies with oscillating dark energy. *Mon. Not. Roy. Astron. Soc.*, 422:1186–1202, 2012.

[12] L. Raul Abramo, Ronaldo C. Batista, and Rogerio Rosenfeld. The signature of dark energy perturbations in galaxy cluster surveys. *JCAP*, 07:040, 2009.

[13] A. Mehrabi, S. Basilakos, and F. Pace. How clustering dark energy affects matter perturbations. *Mon. Not. Roy. Astron. Soc.*, 452(3):2930–2939, 2015.

[14] Francesco Pace, Sven Meyer, and Matthias Bartelmann. On the implementation of the spherical collapse model for dark energy models. *JCAP*, 10:040, 2017.

[15] Francis Bernardeau. Skewness and Kurtosis in large scale cosmic fields. *Astrophys. J.*, 433:1, 1994.

[16] F. Bernardeau, S. Colombi, E. Gaztanaga, and R. Scoccimarro. Large scale structure of the universe and cosmological perturbation theory. *Phys. Rept.*, 367:1–248, 2002.

[17] P. J. E. Peebles. *The large-scale structure of the universe*. 1980.

[18] Hermano Velten and Raquel Emy Fazolo. Skewness of matter distribution in clustering dark energy cosmologies. *Phys. Rev. D*, 101(2):023518, 2020.

[19] R. R. R. Reis, M. Makler, and Ioav Waga. Skewness as a test for quartessence. *Phys. Rev. D*, 69:101301, 2004.

[20] M. Wolk, H. J. McCracken, S. Colombi, J. N. Fry, M. Kilbinger, P. Hudelot, Y. Mellier, and O. Ilbert. Evolution of hierarchical clustering in the CFHTLS-Wide since $z \sim 1$. *Mon. Not. Roy. Astron. Soc.*, 435:2, 2013.

[21] Luca Amendola et al. Cosmology and fundamental physics with the Euclid satellite. *Living Rev. Rel.*, 21(1):2, 2018.

[22] R. Laureijs et al. Euclid Definition Study Report. 10 2011.

[23] Jaan Einasto, Anatoly Klypin, Gert Hütsi, L. J. Liivamägi, and Maret Einasto. Evolution of skewness and kurtosis of cosmic density fields. *Astron. Astrophys.*, 652:A94, 2021.

[24] J. A. S. Lima, V. Zanchin, and Robert H. Brandenberger. On the Newtonian cosmology equations with pressure. *Mon. Not. Roy. Astron. Soc.*, 291:L1–L4, 1997.

[25] R. R. R. Reis. Domain of validity of the evolution of perturbations in Newtonian cosmology with pressure. *Phys. Rev. D*, 67:087301, 2003. [Erratum: *Phys. Rev. D* 68, 089901 (2003)].

[26] Adam Moss, Edmund Copeland, Steven Bamford, and Thomas Clarke. A model-independent reconstruction of dark energy to very high redshift. 9 2021.

[27] R. R. Caldwell. A Phantom menace? *Phys. Lett. B*, 545:23–29, 2002.

[28] K. Benabed and F. Bernardeau. Testing quintessence models with large scale structure growth. *Phys. Rev. D*, 64:083501, 2001.

- [29] Olga Sergijenko and Bohdan Novosyadlyj. Sound speed of scalar field dark energy: weak effects and large uncertainties. *Phys. Rev. D*, 91(8):083007, 2015.
- [30] Tobias Basse, Ole Eggers Bjaelde, and Yvonne Y. Y. Wong. Spherical collapse of dark energy with an arbitrary sound speed. *JCAP*, 10:038, 2011.
- [31] Paolo Creminelli, Guido D'Amico, Jorge Norena, Leonardo Senatore, and Filippo Vernizzi. Spherical collapse in quintessence models with zero speed of sound. *JCAP*, 03:027, 2010.
- [32] J. N. Fry and Enrique Gaztanaga. Biasing and Hierarchical Statistics in Large-Scale Structure. *Astrophys. J.*, 413:447, August 1993.
- [33] F. Bernardeau, R. Juszkiewicz, A. Dekel, and F. R. Bouchet. Omega from the skewness of the cosmic velocity divergence. *Mon. Not. Roy. Astron. Soc.*, 274:20–26, 1995.
- [34] R. Juszkiewicz, F. R. Bouchet, and S. Colombi. Skewness induced by gravity. *Astrophys. J. Lett.*, 412:L9, 1993.
- [35] Luca Amendola and Claudia Quercellini. Skewness as a Test of the Equivalence Principle. *Phys. Rev. Lett.*, 92(18):181102, May 2004.
- [36] Takayuki Tatekawa and Shinji Tsujikawa. Second-order matter density perturbations and skewness in scalar-tensor modified gravity models. *JCAP*, 09:009, 2008.